Sains Malaysiana 51(4)(2022): 1197-1212
http://doi.org/10.17576/jsm-2022-5104-20

Microwave Synthesis of Blue Emissive N-Doped Carbon Quantum Dots as a Fluorescent Probe for Free Chlorine Detection

(Sintesis Gelombang Mikro N-Terdop Titik Kuantum Karbon Pancaran Biru sebagai Prob Pendarfluor untuk Pengesanan Klorin Bebas)

MELISSA ASHA LARSSON[1], PRAVENA RAMACHANDRAN[1], PURIM JARUJAMRUS[2,3] & HOOI LING LEE[1*]

[1]Nanomaterials Research Group, School of Chemical Sciences, Universiti Sains Malaysia, 11800 USM, Penang, Malaysia
[2]Department of Chemistry and Centre of Excellence for Innovation in Chemistry, Faculty of Science, Ubon Ratchathani University, Ubon Ratchathani, Thailand
[3]Nanomaterials Science, Sensors & Catalysis for Problem-Based Projects, Faculty of Science, Ubon Ratchathani University, Ubon Ratchathani, Thailand

Received: 8 June 2021/Accepted: 8 September 2021

ABSTRACT

Blue emissive N-doped carbon quantum dots (N-CQDs) were prepared through a convenient and sustainable microwave synthesis method using citric acid monohydrate (CA) and urea as carbon and nitrogen sources, respectively, with an optimum molar ratio of 1:3 (CA:Urea). The surface functional groups, morphology, and hydrodynamic characteristics of N-CQDs were analysed with Fourier-transform infrared (FTIR) spectroscopy, high-resolution transmission electron microscopy (HRTEM) and dynamic light scattering (DLS), respectively. The as-synthesised N-CQDs with a quantum yield of 14.8%, exhibited excitation-independent fluorescence emission at 443 nm due to surface-state-induced fluorescence, with an optimum excitation wavelength at 360 nm. The N-CQDs were spherical, with an average particle size of 7.29 ± 3.91 nm based on HRTEM analysis. However, DLS analysis showed that the hydrodynamic size (293.0 ± 110.8 nm) was larger than the average particle size due to the presence of hydrophilic polymer chains and abundant surface groups on the N-CQDs. The free chorine-induced fluorescence quenching of N-CQDs at pH 9 denotes the sensitivity of N-CQDs towards detection of free chlorine in the form of hypochlorite (ClO^-) ion, providing the limit of detection (LOD) of 0.4 mM and limit of quantification (LOQ) of 1.2 mM. The fluorescence quenching effect in the N-CQDs caused by the quencher (ClO^-) is attributed to the dynamic quenching mechanism, via an intersystem crossing. The low selectivity of N-CQDs towards various ions justified N-CQDs' selectivity as a free chlorine fluorescent probe that can be used for wastewater testing due to its high range sensitivity.

Keywords: Fluorescent probe; free chlorine detection; microwave synthesis; N-doped carbon quantum dots (N-CQDs)

ABSTRAK

Pancaran biru titik kuantum karbon terdop N (N-CQDs) telah disediakan melalui kaedah gelombang mikro yang mudah dan lestari dengan menggunakan asid sitrik monohidrat (CA) dan urea masing-masing sebagai sumber karbon dan nitrogen dengan nisbah molar optimum 1:3 (CA:Urea). Kumpulan berfungsi permukaan, morfologi dan ciri hidrodinamik N-CQDs telah dianalisis dengan spektroskopi transformasi Fourier inframerah (FTIR), mikroskop pancaran elektron resolusi tinggi (HRTEM) dan penyerakan cahaya dinamik (DLS), masing-masing. N-CQDs yang disintesis dengan 14.8% hasil kuantum telah mengeluarkan pelepasan pendarfluor pengujaan-bebas pada 443 nm disebabkan pendarfluor teraruh keadaan permukaan dengan gelombang pengujaan optimum pada 360 nm. N-CQDs adalah berbentuk sfera dengan purata saiz zarah 7.29 ± 3.91 nm berdasarkan analisis HRTEM. Namun, analisis DLS telah menunjukkan bahawa saiz hidrodinamik (293.0 ± 110.8 nm) adalah lebih besar daripada purata saiz zarah disebabkan kehadiran rantaian polimer hidrofil dan banyak kumpulan berfungsi permukaan pada N-CQDs. Lindapan pendarfluor N-CQDs teraruh klorin bebas pada pH 9 menunjukkan kepekaan N-CQDs terhadap pengesanan klorin bebas dalam bentuk ion hipoklorit (ClO^-), yang memberi had pengesanan (LOD) 0.4 mM dan had pengkuantitian (LOQ) 1.2 mM. Kesan

lindapan pendarfluor di N-CQDs yang disebabkan oleh pelindap (ClO^-) adalah dikaitkan dengan mekanisme lindapan dinamik, melalui lintasan antara sistem. Kepekaan N-CQDs yang rendah terhadap beberapa ion mewajarkan keterpilihan N-CQDs sebagai prob pendarfluor klorin bebas yang boleh digunakan bagi pengujian air sisa disebabkan julat kepekaan yang tinggi.

Kata kunci: Pengesanan klorin bebas; prob pendarfluor; sintesis gelombang mikro; titik kuantum karbon terdop N-CQDs

INTRODUCTION

Molecular chlorine (Cl_2), hypochlorous acid (HClO), and hypochlorite (ClO^-) are notable disinfectants used by more than 80% of waterworks such as water treatment and home-bleaching solutions (Emmanuel et al. 2004). The combination of Cl_2, HClO, and ClO^- in aqueous form is known as free chlorine, and their dominant presence depends on the pH of water. Free chlorine is a useful disinfectant worldwide, as it is also used in water reuse standards, such as in the USA (Crook et al. 2012). Therefore, there is no doubt that free chlorine has numerous advantages. Nevertheless, it is important to regulate free chlorine levels below the standard requirement depending on its application, to avoid adverse effects on human beings, animals and the environment. The National Institute for Occupational Safety and Health (NIOSH) stated that the Immediately Dangerous to Life or Health Concentrations (IDLH) of free chlorine is 10 ppm (0.13 mM) (National Institute for Occupational Safety and Health 1997). Moreover, immoderate-free chlorine reacts with organic compounds existing in water to form numerous carcinogens, such as trihalomethanes (THMs) (Yee et al. 2006). Therefore, it is important to monitor and control the free chlorine level in the samples tested to prevent free chlorine pollution in the environment.

Several analytical methods were discovered for free chlorine detection in the past, such as iodometric titration (Heidelberger & Treffers 1942), ion chromatography (Chen et al. 1999), gas chromatography (Wakigawa et al. 2013), liquid chromatography (Wakigawa et al. 2013), and flow injection analysis (Watanabe et al. 1998). Free chlorine detection has also been explored by synthesising probes for free chlorine detection. The summary of different free chlorine detection methods using different probes is depicted in Table 1. For example, a colorimetric method was developed using gold/silver alloy nanoparticles (Au/Ag alloy NP) that were synthesised using tetrachloroauric (III) acid ($HAuCl_4$), silver nitrate ($AgNO_3$), and trisodium citrate via reflux. These nanoparticles detected free chlorine with a LOD of 0.3 μM (Shanmugaraj & Ilanchelian 2017). Yuan et al. (2016) utilised fluorescence quenching method by employing 1-pyrenylboronic acid to detect free chlorine and this method has a LOD of 0.21 μM. In addition, free chlorine detection was also reported using fluorescent dye Nile blue A, which has a LOD of 0.04 μM (Duan et al. 2015). Besides, Yadav et al. (2019) successfully produced 2-[(2-amino-5-nitro-phenyl-amino)-methyl]-5-diethylamino-phenol (L1), a complex compound to detect free chlorine with a LOD of 4.60 μM. Although each above-mentioned method has its advantages, these methods have limitations related to detection sensitivity, selectivity, use of toxic materials, and complicated procedures.

TABLE 1. Comparisons of various free chlorine detection methods

Method	Probe	LOD (μM)	Reference
Colorimetry	Gold/silver alloy nanoparticles (Au/Ag alloy NP)	0.3	Shanmugaraj & Ilanchelian (2017)
Fluorescence quenching method	1-pyrenylboronic acid	0.21	Yuan et al. (2016)
Electrochemical analysis	Ferrocene compounds (several)	1-50	Wang & Anzai (2015)
Fluorescence quenching method	Nile blue A	0.04	Duan et al. (2015)
Fluorescence quenching method	2-[(2-amino-5-nitro-phenyl-amino)-methyl]-5-diethylamino-phenol (L1)	4.60	Yadav et al. (2019)

In this regard, fluorometry is observed as a promising technique to address the shortcomings in terms of sensitivity and selectivity. Moreover, fluorescent probes serve an advantage for real-time monitoring. Organic dyes such as rhodamine (Pobozy et al. 1995) and fluorescein (Koide et al. 2011) have been developed as organic fluorescent probes due to the advantages associated with their low toxicity and they are relatively inexpensive; however, they have low photobleaching resistance. These shortcomings can be solved by semiconductor quantum dots (QDs), as they exhibit excellent photophysical properties compared to organic dyes. Examples of notable QDs used are metal chalcogenides such as CdS, CdTe, PbSe, and PbS, but the heavy metal content in these QDs induces toxicity that significantly limits their application. Due to these limitations, researchers have started to explore carbon quantum dots (CQDs) because of their diverse structures and variety of fluorescence properties (De Medeiros et al. 2019; Shepherd et al. 2007). CQDs are better substitutes than other semiconductor quantum dots from an environmental perspective because of their good fluorescence properties, good biocompatibility, low toxicity, the flexibility of synthesis precursors, and method of synthesis (Du & Guo 2016), thus, making them a desirable fluorescent probe. Another advantage of CQDs is their fluorescence properties; highly dependent on the surface state, which is easily adjustable by varying precursors, reaction parameters, method of synthesis, and dispersing solvents (Shepherd et al. 2007). Besides, N-CQDs have a strong ability to bind with molecules attributed to their abundant surface groups such as carboxyl, carbonyl, amine, amide, and hydroxyl groups, as well as pyridinic nitrogen and pyrrolic nitrogen. Hence, the efficiency of recombination of the electron-hole pairs can be changed, which could alter the fluorescent emissions of the N-CQDs (Qu et al. 2015). It has been reported that doping of heteroatoms (N atom) into CQDs enhances their quantum yield and fluorescence emission intensity (De Medeiros et al. 2019). The presence of dopants with extra lone pairs of electrons enriches electron delocalisation. It increases surface defects in the CQDs as more electrons contribute to the surface of the CQDs' carbon core (surface state). They were reported to be very good selective fluorescent probes for detecting various ions, such as heavy metals, cations, and anions (Lou et al. 2015), as their surface state reacts differently with the target ion compared to the others. Commonly, CQDs can be used as fluorescent probes employing fluorescence quenching when in contact with target ions. Numerous mechanisms contribute to fluorescence quenching, namely static quenching, dynamic quenching, energy transfer, inner filter effect (IFE), and photoinduced electron transfer (PET) (Zu et al. 2017). Nevertheless, static and dynamic quenching are generally compared before advancing further to other mechanisms (Bunkoed & Kanatharana 2015; Lakowicz 1999; Yu et al. 2003). Static quenching is attributed to a non-fluorescent ground state complex formation through the CQDs-quencher interaction. Meanwhile, dynamic quenching involves the collision between CQDs and quencher, which results in the excited state of the CQDs returning to the ground state following the energy transfer or charge transfer mechanism. The theory of fluorescence quenching can be complex, hence further research on this topic may lead to many discoveries.

The method of synthesis of CQDs must be considered seriously as it affects the surface structure of these CQDs. Arc-discharge, laser ablation, and electrochemical methods are prominent conventional methods used for CQDs syntheses (Liu et al. 2019; Yoo et al. 2019). Unfortunately, these methods are expensive, use harmful reagents, require many steps, and have a long duration of CQDs synthesis. Unsustainable precursors with hard accessibility are often used in these methods. Although the hydrothermal process is environmentally friendly, it requires a long duration for CQDs synthesis. On the other hand, microwave synthesis is a sustainable, rapid, and simple method for CQDs synthesis compared to the stated methods. This method requires a shorter duration and a single step to synthesise CQDs with a high quantum yield. Besides, this method is eco-friendly and can utilise simple precursors for synthesis (Shepherd et al. 2007).

In this study, a green and facile microwave synthesis of N-CQDs using citric acid monohydrate (source of carbon) and urea (source of nitrogen). This is a simple, fast, selective, and sensitive N-CQDs-based fluorescent probe technique that was developed to detect free chlorine. The mechanism of the use of N-CQDs as a fluorescent probe in this work was also investigated. Ultimately, the proposed fluorescent probe can serve as a promising sensor for developing an efficient fluorometric sensor for detecting free chlorine.

Materials and Methods

Materials

Citric acid monohydrate (QREC (Asia) Sdn. Bhd., Malaysia), urea (Merck KGaA Germany), sodium hypochlorite (BHD Chemicals Ltd England, UK), magnesium chloride hexahydrate (Sigma-Aldrich Co. USA), manganese sulfate monohydrate (Sigma-

Aldrich Co. USA), calcium chloride (Orioner Hightech Sdn. Bhd, Malaysia), ammonium chloride (Orioner Hightech Sdn. Bhd., Malaysia), sulphuric acid (H_2SO_4, 95-97% QREC (Asia) Sdn. Bhd., Malaysia), cadmium chloride monohydrate (Merck KGaA, Germany), sodium hydroxide (Merck KGaA, Germany), quinine sulfate dihydrate (Acros Organics, USA), hydrochloric acid (HCl, 37%, QREC (Asia) Sdn. Bhd., Malaysia). Deionised water was used to prepare all solutions. All chemicals used were of analytical grade without further purification.

PREPARATION OF N-CQDS

Microwave synthesis of N-CQDs was prepared with some modifications from Sun et al. (2018). Firstly, 0.0048 mol of citric acid monohydrate and 0.0143 mol of urea were dissolved in 12.5 mL of deionised water. The molar ratio of citric acid monohydrate to urea (CA:Urea) used was 1:3. A constant magnetic stirring of the mixture was applied for 5 min. The mixed transparent solution was then transferred to a 100 mL-sealed vessel made of high-purity modified Teflon (TFM), placed in a synthesis microwave (Milestone flexiWAVE, Milestone Inc. (USA)), and subjected to microwave irradiation power of 750 W. The temperature and duration of irradiation settings were 200 °C and 5 min, respectively. Finally, the prepared sample was centrifuged at 10,000 rpm for 5 min to attain purified liquid N-CQDs.

QUANTUM YIELD (QY) OF N-CQDS

The QY of N-CQDs (sample) was determined by comparing the integrated fluorescence (FL) intensities and the absorbance value of the sample and quinine sulphate (standard). The quinine sulphate (Q_{st}= 0.54 at an excitation wavelength of 360 nm) was prepared in 0.1 M H_2SO_4 (η_{st}= 1.33). Meanwhile, N-CQDs were dissolved in deionised water (η_x=1.33). The absorbance of the sample was kept under 0.1 at the excitation wavelength. The QY of the N-CQDs was calculated using (1):

$$Q_x = Q_{st}\left(\frac{M_x}{M_{st}}\right)\left(\frac{\eta_x}{\eta_{st}}\right)^2 \quad (1)$$

where Q is the quantum yield; M is the gradient from the linear regression; and η is the refractive index of the solution. The subscripts 'x' and 'st' refer to the sample and standard fluorescent agent (quinine sulphate), respectively.

CHARACTERISATIONS

The absorbance spectra of N-CQDs were obtained using a double-beamed UV-2600 UV-Vis spectrophotometer (Shimadzu, Japan) between the wavelength range of 200-800 nm. Further optical characterisation was conducted via PERKIN ELMER LS 55 Luminescence Spectrometer (USA) at a wavelength range of 300-700 nm to determine fluorescence (FL) properties of the N-CQDs. Fourier transform infrared (FTIR) spectra of the sample were recorded by the ATR method on PerkinElmer Frontier FT-NIR Spectrometer Frontier (USA) in the range of 600-4000 cm^{-1}. The size and morphology of the as-synthesised N-CQDs were performed using High-Resolution Transmission Electron Microscope (HRTEM) 200 kV with Field Emission, TECNAI G2 20 S-TWIN, FEI (Spain). Malvern Zetasizer Nano ZS (UK) was used to determine the hydrodynamic size and mean zeta potential of the N-CQDs dispersed in deionised water.

DETERMINATION OF FREE CHLORINE IN DEIONISED WATER

A 0.01 M stock solution of sodium hypochlorite (NaOCl) was employed throughout this study. An optimum excitation wavelength of 360 nm was selected for the determination of fluorescence intensity throughout this section.

DETECTION OF FREE CHLORINE CONCENTRATION IN DEIONISED WATER

10 µL of N-CQDs was added to five 10 mL volumetric flasks. Concentrations of 1, 2, 3, 4, and 5 mM from the stock solution were added to the five flasks, respectively. Then, the final volume of 10 mL was adjusted with a solution of pH 9. After 30 min, the fluorescence spectra of the solutions were obtained. Lastly, a calibration curve (average values from triplicate measurements) was plotted between the ratio of blank fluorescence intensity/fluorescence intensity with added OCl^- (I_o/I) against OCl^- concentration in mM. The LOD and LOQ were calculated from the obtained calibration curve, using (2) and (3).

$$LOD = 3.3*SD_{blank} / slope \quad (2)$$

$$LOQ = 10*SD_{blank} / slope \quad (3)$$

To obtain an optimum duration and pH to detect

free chlorine concentration in deionised water, the effect of these parameters was studied as explained in the following subsections.

EFFECT OF DURATION

10 µL of N-CQDs was added to a 10 mL volumetric flask. Then, 5 mM from the stock solution was added to the flask. The solution was topped up to the 10 mL calibration mark with a solution of pH 9. Then, the fluorescence spectra of the prepared solution were obtained at intervals of 1 min for 35 min. The maximum fluorescence intensities of each spectrum were noted. Finally, a curve was plotted between fluorescence intensity against time. The optimum duration is noted where the fluorescence intensity begins to remain constant. This duration is used throughout the determination of free chlorine.

EFFECT OF PH

The steps for the addition of N-CQDs and NaOCl stock solution to 10 mL volumetric flask under the last subsection are repeated in this subsection with 11 separate flasks. Each flask was topped up to the 10 mL calibration mark with solutions of pH values 2, 3, 4, 5, 6, 7, 8, 9, 10, 11, and 12. The acidity and basicity of solutions were adjusted using hydrochloric acid (HCl) and sodium hydroxide (NaOH), respectively. Then, the fluorescence spectra of the prepared solutions were obtained after 30 min. Lastly, a curve was plotted between the difference of blank fluorescence intensity and fluorescence intensity with added OCl^- (I_o-I) against the pH of solutions. The optimum pH is noted where I_o-I had the highest value.

SELECTIVITY OF N-CQDS TOWARDS OTHER IONS

The selectivity of N-CQDs for several ions was evaluated at pH 9. This experiment proved that the selectivity of N-CQDs towards free chlorine is the most sensitive compared to other ions. The ions tested were Cd^{2+}, Ca^{2+}, Mg^{2+}, Mn^{2+}, and NH_4^+. A fixed amount of 10 µL of N-CQDs was added to all the volumetric flasks. 5 mM of the different ions, including free chlorine, were added to a series of 10 mL volumetric flasks, separately. The level was topped up to the calibration mark with a solution of pH 9. After 30 min, the fluorescence spectra of the prepared samples were recorded. This method was executed three times to obtain triplicate measurements, where the average value of fluorescence intensity with added ion was denoted as I. A graph was plotted between the difference between blank fluorescence intensity and fluorescence intensity with added ion (I_o-I) against the type of ions.

The methods for the detection of free chlorine in deionised water was repeated for concentrations 1, 3, and 5 mM, five times in one day and for five consecutive days to determine the intra-day and inter-day precision, respectively.

Results and Discussion

FOURIER-TRANSFORM INFRARED SPECTROSCOPY (FTIR)

FTIR spectroscopy was performed to identify the surface functional groups present on the N-CQDs. Figure 1 shows the FTIR spectrum of (a) citric acid monohydrate (b) urea and (c) N-CQDs. The peak at 3174 and 2836 cm^{-1} in the N-CQDs corresponds to the O-H bond stretching from hydroxyl groups and C-H stretching, respectively. The peaks at 1548 and 1432 cm^{-1} are attributed to the N-H stretching of the amine group and the bending vibrations of C-N of the amine group from urea, respectively. These two peaks are also apparent in N-CQDs, which proves the presence of surface amine groups of the N-CQDs is from urea. The peak at 1296 cm^{-1} in the N-CQDs relates to the C-N stretching of aromatic amines. This finding suggests that nitrogen atom has been doped to the carbon core of N-CQDs. Stretching vibration of C–O from tertiary alcohol appears at 1179 cm^{-1} in the N-CQDs FTIR spectrum. This observation may be due to the bonding of the -OH group from citric acid to the carbon core (consisting of many carbon-carbon bondings) of N-CQDs. The peak at 1655 cm^{-1} is assigned to the stretching vibrations of C=O, which is present in CA and the N-CQDs. The presence of C=O stretching vibrations and C-N bending vibrations suggest the presence of amide groups. It is important to note that the intensity of the bending vibrations of N-H (1548 cm^{-1}) is stronger than the characteristic C=O stretching (1655 cm^{-1}), which suggests that the microwave synthesis of N-CQDs from urea and CA has resulted in more abundant amine groups on the surface from urea, compared to existing carbonyl groups from CA (Sun et al. 2018). The evidence of the presence of amine and carbonyl groups (good hydrophilicity) through FTIR analysis explains the solubility of N-CQDs in deionised water.

The FTIR analysis of CA, urea, and N-CQDs, confirms the presence of amine, amide, carboxyl,

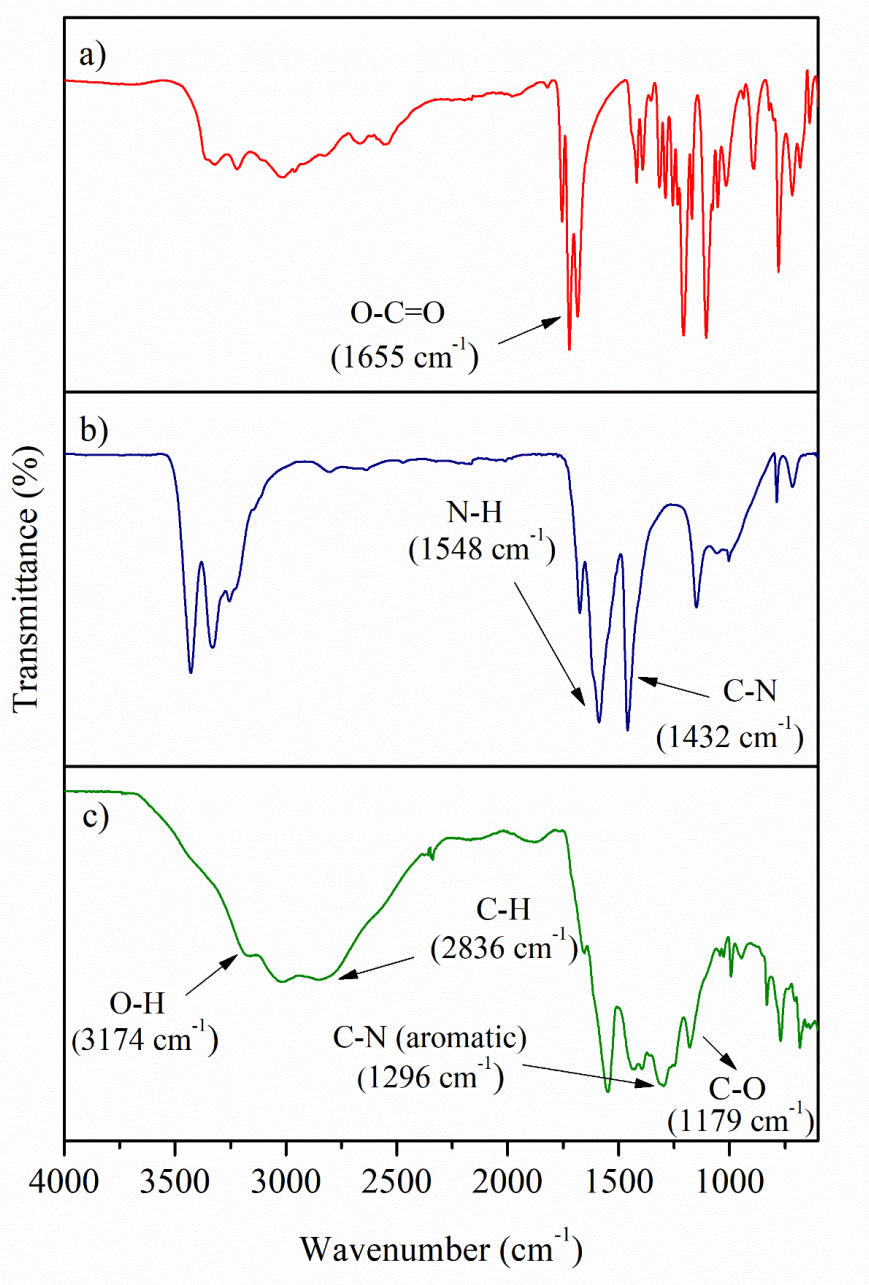

FIGURE 1. FTIR spectra of (a) citric acid monohydrate, (b) urea, and (c) N-CQDs

carbonyl, and hydroxyl groups on the N-CQDs' surface. Besides, there is evidence of nitrogen doping of the N-CQDs due to the presence of aromatic nitrogen. Each functional group plays an important role involving the fluorescence properties of N-CQDs, as explained in the earlier subsections.

HIGH-RESOLUTION TRANSMISSION ELECTRON MICROSCOPY (HRTEM)

The size and morphology of the as-synthesised N-CQDs were carried out using HRTEM. Figure 2 shows (a) HRTEM image of the N-CQDs and (b) distribution of particle diameters of N-CQDs based on HRTEM analysis. Based on Figure 2(a), it can be confirmed that the carbon-based particles analysed are quantum dots due to their particle size that is less than 10 nm and they are in spherical shapes. From Figure 2(b), the average particle size of

the N-CQDs is 7.29 ± 3.91 nm. There is a presence of particle sizes that range of more than 10 nm, which might be due to the agglomeration of N-CQDs that resulted from drying the sample before HRTEM analysis. The presence of lattice fringes in the HRTEM image indicates the crystallisation process of the N-CQDs under microwave irradiation. However, the absence of distinguishable fringes may suggest the presence of amorphous regions

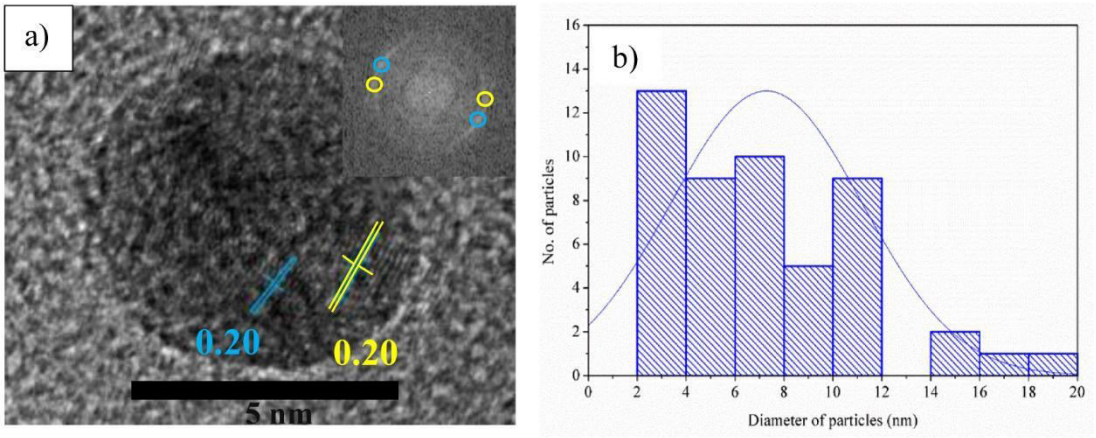

FIGURE 2. (a) HRTEM image of the N-CQDs and (b) the distribution of particle diameters of N-CQDs based on HRTEM analysis

(Kim et al. 2015). Based on literature studies, CQDs exhibit lattice fringes with a d-spacing of 0.20 nm (Liu et al. 2017), whereas GQDs have an additional d-spacing of 0.34 nm (Qin et al. 2019). Therefore, it can be confirmed that the obtained quantum dots are CQDs in which all lattice fringes have a d-spacing of 0.20 nm. This spacing is associated with the (100) in-plane lattice spacing of graphite (Ding et al. 2016).

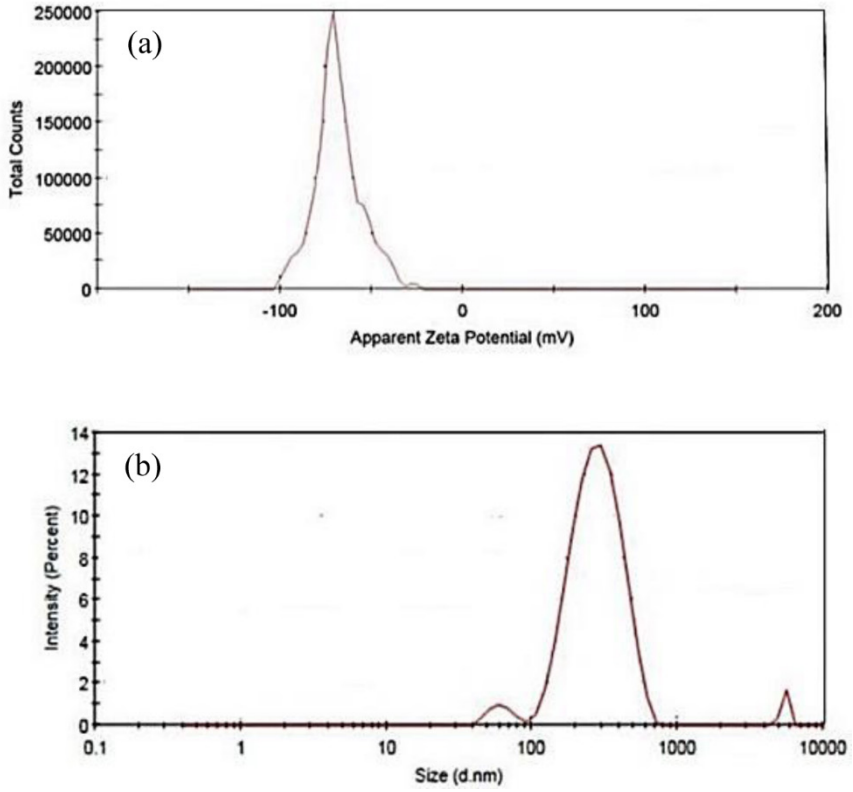

FIGURE 3. (a) DLS spectrum of size distribution by the intensity and (b) mean zeta potential distribution of N-CQDs diluted in deionised water (1:1000)

DYNAMIC LIGHT SCATTERING (DLS)

The hydrodynamic size and mean zeta potential of the obtained N-CQDs dispersed in deionised water were determined. Figure 3(a) shows the DLS hydrodynamic size distribution by the intensity with a dilution of N-CQDs in deionised water (1:1000). The hydrodynamic size distribution of the N-CQDs is 293.0 ± 110.8 nm, which is much larger than the average particle size of the N-CQDs (7.29 ± 3.91 nm), as calculated based on the HRTEM results. Factors that caused overestimated hydrodynamic size include polydispersity, ionic strength of the medium, and surface structure of N-CQDs (Kaasalainen et al. 2017; Malvern Panalytical Ltd. 2018). However, the polydispersity factor is ruled out since the Polydispersity Index (PDI) of 0.307 proved that the N-CQDs are monodispersed in deionised water. The second factor is neglected because ion concentrations in deionised water are insignificant. Therefore, the large difference in the average particle size measured between the DLS and HRTEM results may be attributed to the complex surface structure of the N-CQDs. Apart from functional groups, the surface of the N-CQDs may consist of hydrophilic polymeric structures that extend when N-CQDs are dispersed in deionised water. This surface characteristic is usually caused by incomplete carbonisation of polymer chains during bottom-up thermal synthesis of N-CQDs (Xia et al. 2019).

The mean zeta potential distribution of the N-CQDs in deionised water is measured to be −68.6 ± 12.5 mV, as shown in Figure 3(b). The finding suggests that the surface of N-CQDs is negatively charged as there is high electron cloud density around the N-CQDs due to numerous electrons from the doping of nitrogen, thereby resulting in good colloidal stability (Ding & Xiong 2015). With good colloidal stability, it is confirmed that there is no agglomeration of N-CQDs when dispersed in deionised water.

OPTICAL PROPERTIES OF N-CQDS

The UV-Vis and FL spectra of N-CQDs dispersed in deionised water (1:1000) are illustrated in Figure 4(a) and 4(b), respectively. N-CQDs have strong absorptions in the ultraviolet region. The UV-Vis spectrum of N-CQDs contains two peaks, namely a peak at 208 nm that is

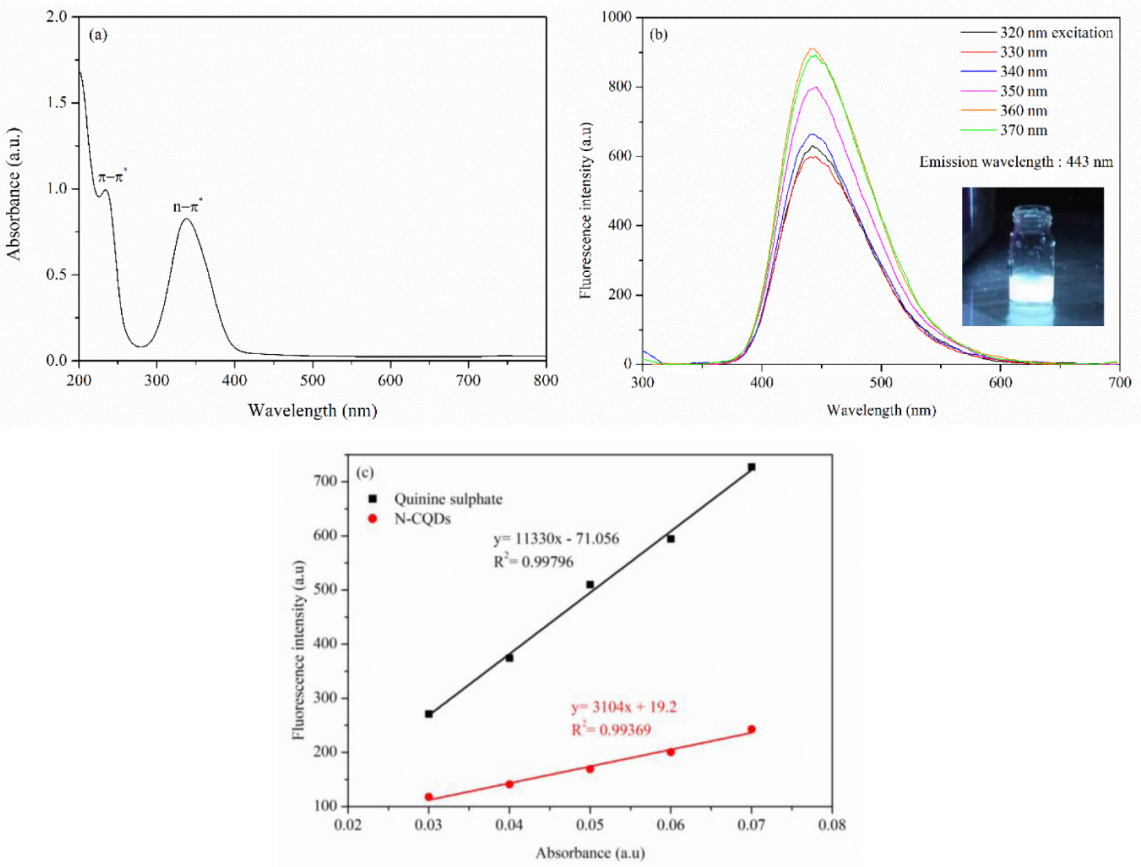

FIGURE 4. (a) UV-Vis spectrum, (b) Fluorescence emission spectra of N-CQDs under several excitation wavelengths after being dispersed in deionised water (1:1000) and inset of the diluted sample irradiated with 365 nm UV light, (c) Fluorescence intensity against UV-Vis absorbance of N-CQDs and quinine sulphate as reference

attributed to the π-π* transition of C=C and bonds within the N-CQDs carbon core structure. Another peak at 340 nm is attributed to the n-π* transition of the aromatic sp^2 system containing C=O and C-N groups. Furthermore, when the N-CQDs were irradiated under 365 nm UV light, they emitted strong blue emissions (Inset of Figure 4(b)). Generally, the peak that corresponds to n-π* transitions determine the excitation wavelength of the fluorescence spectra, and the peak due to π-π* transition does not generate fluorescence (Qin et al. 2019; Zhao & Zhu 2018). Thus, the maximum emission wavelength is deduced by varying the excitation wavelengths (320, 330, 340, 350, 360, and 370 nm). The FL emission spectra of the N-CQDs exhibited excitation-independent fluorescence emission with an optimum FL emission at 443 nm under an excitation wavelength of 360 nm. The excitation-independent fluorescence emission characteristic is a surface states-dominated emission (Zulfajri et al. 2019). Nitrogen doping introduces new surface properties to CQDs and change structural defects, surface functional groups, and intermolecular interactions of the newly doped CQDs (Kalaiyarasan et al. 2019). Therefore, it can be concluded that the presence of surface defects that are passivated due to nitrogen doping, and amine functionalization could be the cause of the excitation-independence of the N-CQDs (Kalaiyarasan et al. 2019; Zulfajri et al. 2019). Besides, the obtained QY results of N-CQDs are depicted in Figure 4(c). Based on the obtained results, the QY of the as-synthesised N-CQDs is 14.8%. This outcome is comparatively higher than other reported synthesis of N-CQDs using citric acid and urea (Simões et al. 2016; Wang et al. 2019).

POSSIBLE FORMATION MECHANISM OF N-CQDS

Figure 5 shows the schematic representation of the chemical reaction between citric acid and urea to form N-CQDs via microwave synthesis. Dehydration and carbonisation of the precursors occurred through heat treatment. Firstly, citric acid and urea were converted to their salts (containing COO^- and NH^{3+}, respectively) after deionised water was added. Next, thermal dehydration of the hydrated salts occurred. This reaction resulted in amide linkage formations to form long polymer chains. These polymeric structures would start to shrink due to continuous intramolecular dehydration as the heating process continued. At this stage, continuous C−C bonds were formed, which led to aromatic clusters

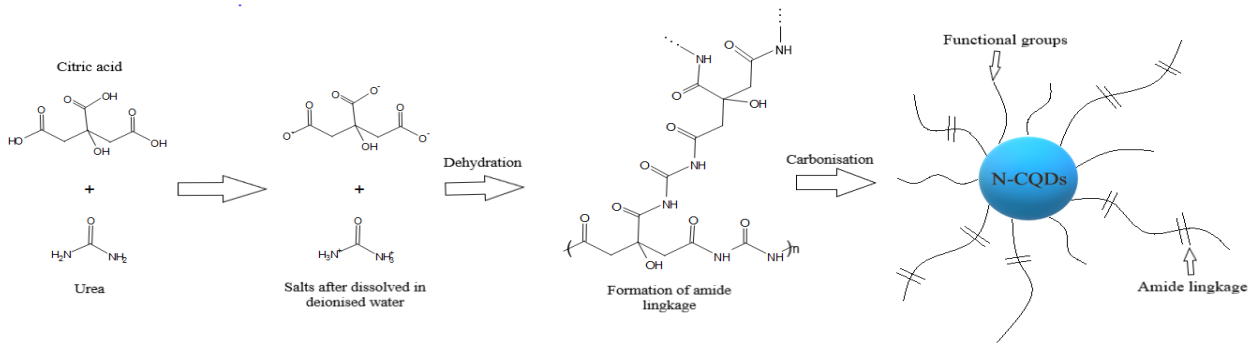

FIGURE 5. Schematic representation of the chemical reaction between citric acid and urea to form N-CQDs *via* microwave synthesis

that were shaped inside the polymers. This was part of the carbonisation process (Yan et al. 2019). This process occurred simultaneously with dehydration until N-CQDs were formed. During carbonisation, nitrogen atoms were being incorporated into the carbon core (nitrogen doping). Due to the possibility of incomplete carbonisation, polymer chains will be present on the surface of the N-CQDs, with other abundant functional groups (Xia et al. 2018). This formation mechanism explains the hydrodynamic size overestimation of the N-CQDs as depicted in Figure 3.

FREE CHLORINE FLUORESCENT PROBE: DETERMINATION OF FREE CHLORINE IN DEIONISED WATER

EFFECT OF DURATION

It is important to monitor the duration-dependent fluorescence changes upon OCl^- addition, to understand the quenching effect of free chlorine on the fluorescence intensity of N-CQDs. Figure 6 shows the effect of duration

towards the quenching effect of the free chlorine on the fluorescence intensity of N-CQDs. As time passed, the fluorescence intensity gradually decreased until it remained constant from 30 min onwards (maximum quenching). Therefore, 30 min was selected as the optimum duration for the detection of free chlorine.

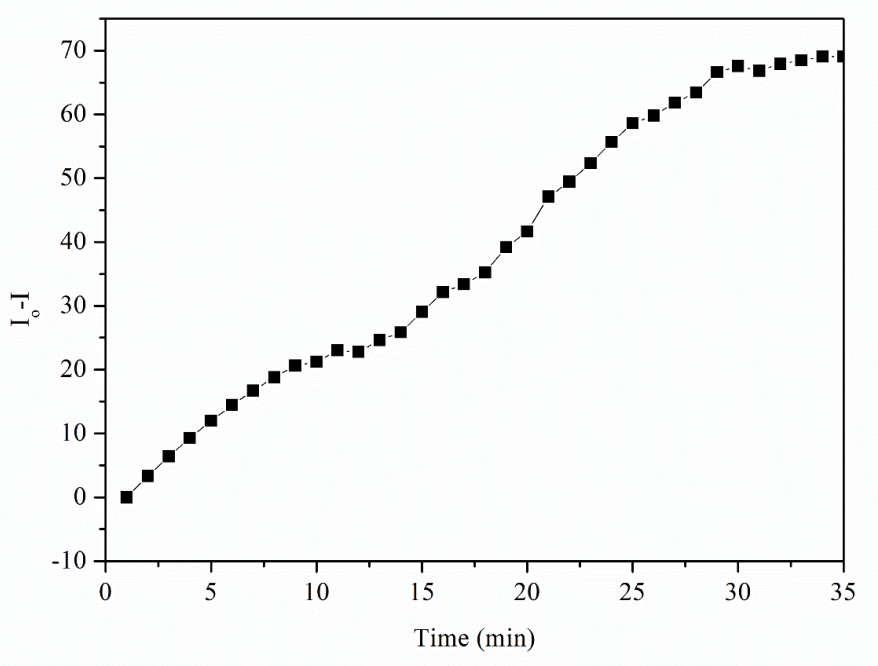

FIGURE 6. Effect of duration towards the quenching effect of the free chlorine on the fluorescence intensity of N-CQDs

EFFECT OF pH

Another important factor that will influence the quenching effect of the N-CQDs is the pH of the solution during the detection of free chlorine because pH value affects the chemical equilibrium between Cl_2, HClO, and ClO^-. Thus, free chlorine will exist as different forms of chlorination chemicals at different pH. Free chlorine exists as Cl_2 below pH 2, while HClO predominates between pH 2 - 7, and above pH 7 equilibrium favours ClO^- in an aqueous medium. Figure 7 shows the effect of pH on the quenching effect of free chlorine on the fluorescence intensity of N-CQDs. It can be deduced that the most suitable pH (highest value of I_o-I) is pH 9. Based on the literature, at pH 9, free chlorine is in the form of ClO^- (Hussain et al. 2015). Therefore, ClO^- has a better quenching effect than Cl_2 and HClO. However, the quenching effect of ClO^- decreased as pH was increased further because of prolonged contact time of ClO^- with the fluorescent probe, leading to poor efficiency in interaction with the functional groups on the surface of the N-CQDs (Zhang et al. 2015).

DETECTION OF FREE CHLORINE CONCENTRATION IN DEIONISED WATER

The analysis for free chlorine detection by N-CQDs in deionised water was performed by constructing a calibration curve (Figure 8) and calculating the LOD and LOQ. From Figure 8, a good linear correlation (R^2 = 0.99598) between the fluorescence intensity ratio (I_o/I) and the concentration of ClO^- (1 - 5 mM) were obtained, which proves that the synthesised N-CQDs can function as a fluorescent probe for detecting free chlorine. The LOD and LOQ were calculated to be 0.4 and 1.2 mM, respectively.

The accuracy and precision of the detection of free chlorine by N-CQDs were determined by performing intra-day and inter-day precision by calculating the difference between the fluorescence intensity of blank and spiked samples of diluted N-CQDs (1:1000), as shown in Table 2. The tabulated data show good intra-day and inter-day

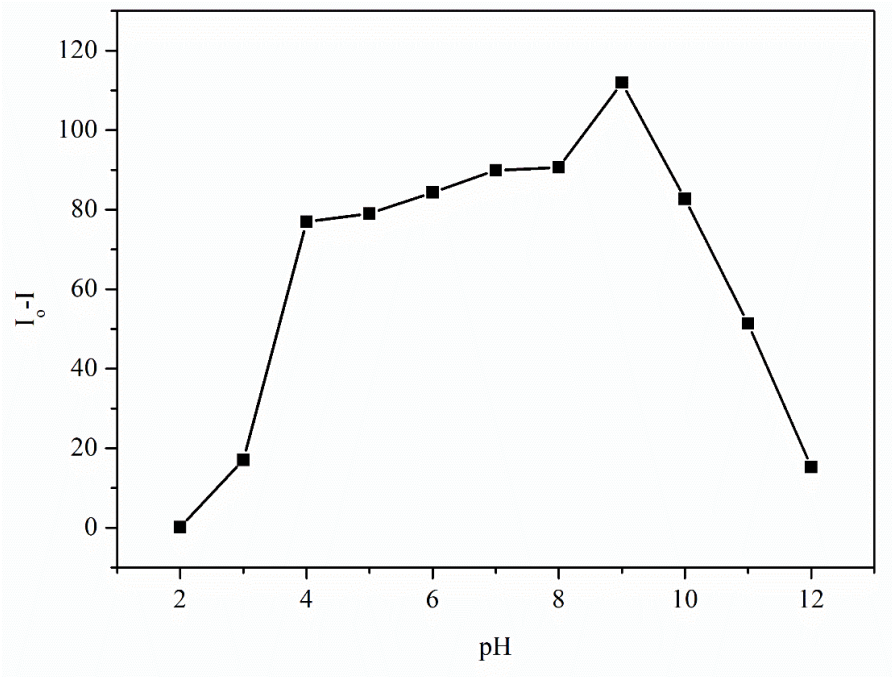

FIGURE 7. Effect of pH towards the quenching effect of free chlorine on the fluorescence intensity of N-CQDs

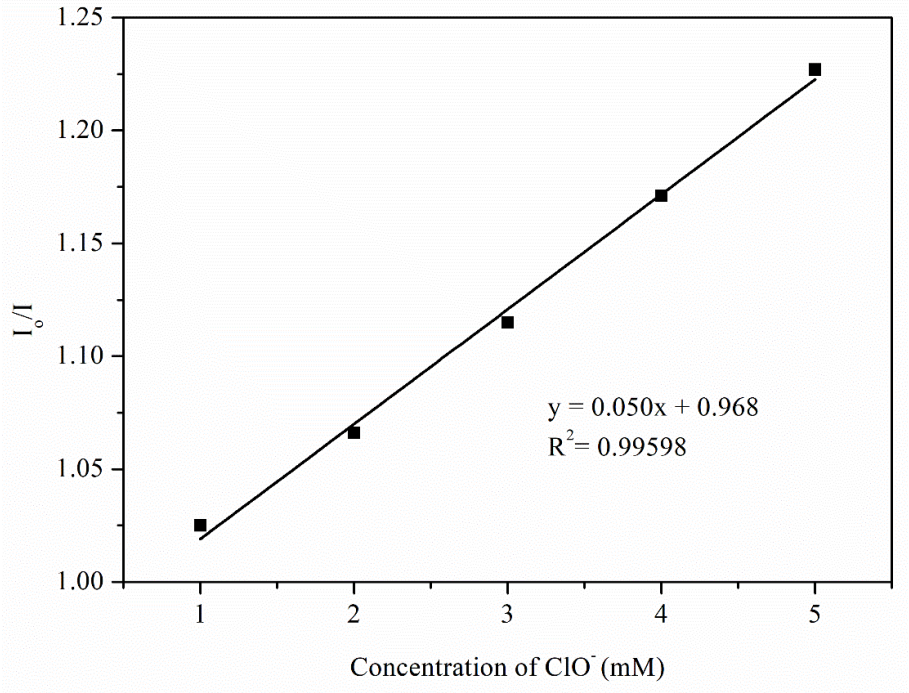

FIGURE 8. Calibration curve of I_o/I against the concentration of ClO^- (mM)

precision with low relative standard deviation (RSD). The average recovery and the corresponding RSD implied a good accuracy of the detection of free chlorine. Therefore, these results justify the moderate efficiency of N-CQDs as a fluorescent probe for the detection of free chlorine.

TABLE 2. Intra-day and inter-day precision determined for different ClO^- concentrations in diluted N-CQDs (1:1000)

	Intra-day precision (n=5)			Inter-day precision (n=5)		
Added (mM)	Found (mM) (Mean ± SD)	Recovery (%)	% RSD	Found (mM) (Mean ± SD)	Recovery (%)	% RSD
1.0	0.996 ± 0.003	99.60	0.30	0.998 ± 0.005	99.80	0.50
3.0	2.998 ± 0.011	99.93	0.37	3.016 ± 0.031	100.5	1.03
5.0	5.014 ± 0.030	100.3	0.60	4.999 ± 0.016	99.98	0.32

SELECTIVITY OF N-CQDS TOWARDS OTHER IONS

The selectivity of N-CQDs was demonstrated using five other ions commonly used for detection (Cd^{2+}, Ca^{2+}, Mg^{2+}, Mn^{2+}, and NH_4^+ ions) and are present in wastewater. The bar chart shown in Figure 9 represents the magnitude of fluorescence quenching (I_o-I) of diluted N-CQDs in the presence of 5 mM of different ions and free chlorine. It was found that the fluorescence quenching of N-CQDs by these other ions is not as significant as that by free chlorine. Therefore, N-CQDs were highly selective in the detection of free chlorine in comparison with other ions.

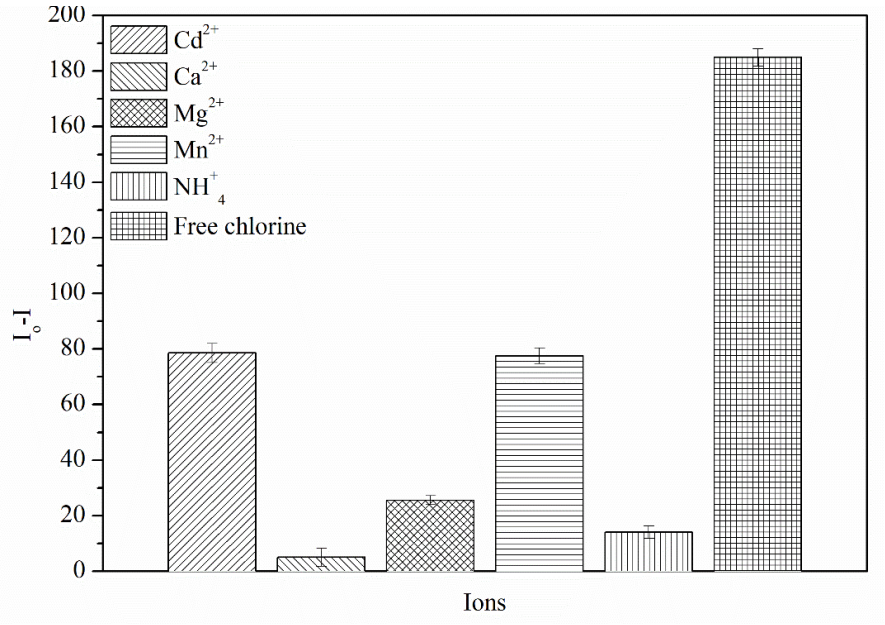

FIGURE 9. The selectivity of N-CQDs towards various ions

THE POSSIBLE FLUORESCENCE QUENCHING MECHANISM

With the addition of NaOCl (source of free chlorine) into a solution of N-CQDs, there was a quenching effect towards the fluorescence intensity of the N-CQDs, as discussed in the free chlorine determination. To determine whether the possible quenching mechanism of ClO^- to the N-CQDs is due to static or dynamic quenching, the Stern–Volmer relationship was studied (4).

$$\frac{I_o}{I} = 1 + K_{SV}[Q] \qquad (1.4)$$

where I_o and I are the fluorescence emission intensity in the absence and presence of ClO^-, respectively. K_{SV} is the Stern-Volmer fluorescence quenching constant, while $[Q]$ is the concentration of the quencher (ClO^-).

Based on the Stern-Volmer plot, the upward curvature as observed in Figure 10(a) illustrates that a combination of static and dynamic quenching occurs in the N-CQDs. Thus, further study was conducted by comparing the UV-Vis spectra of N-CQDs and N-CQDs spiked with ClO^-, as shown in Figure 10(b). The obtained results showed that there was no difference in the UV-Vis spectra of the N-CQDs compared with that of the mixture of N-CQDs and ClO^-. Therefore, this observation confirmed that the quenching process was caused by dynamic quenching, as only the excited states of the N-CQDs were affected. The results also indicate that the N-CQDs and ClO^- did not form a new complex. Moreover, dynamic, or static quenching can be differentiated by performing temperature-dependent quenching studies. The Stern-Volmer plots obtained by varying the temperatures (Figure 10(c)) indicated dynamic quenching increases with an increase in the temperature. Generally, when the temperature increases, the collision frequency between ClO^- and N-CQDs increases. Hence, the rise in dynamic quenching with temperature can be ascribed to its dynamic (collision) nature (Song et al. 2014). This finding further verifies that the fluorescence quenching effect in the N-CQDs

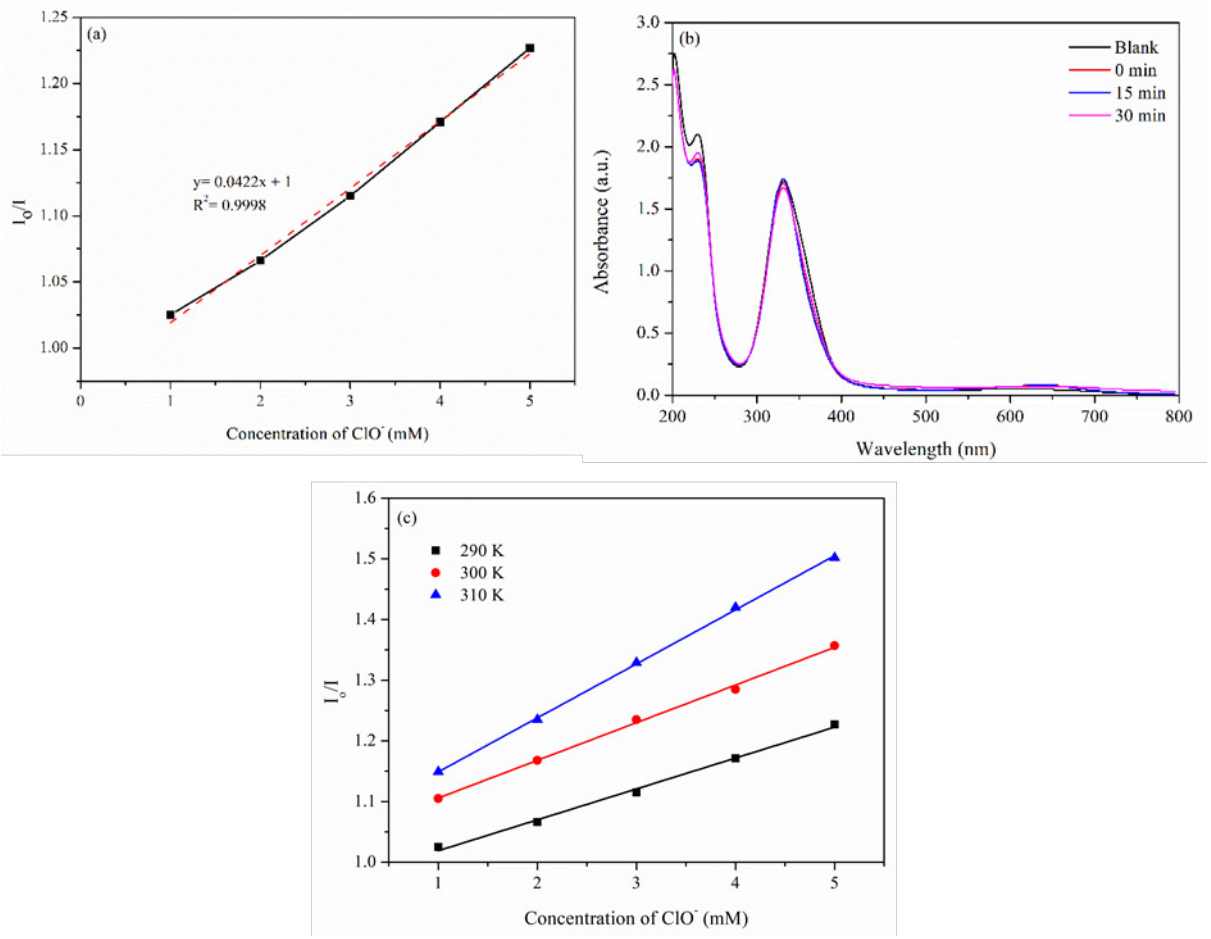

FIGURE 10. (a) The Stern – Volmer plot for the interaction of ClO^- and the N-CQDs at different concentrations, (b) UV-Vis spectrum of N-CQDs and N-CQDs spiked with ClO^- at different durations, (c) Stern – Volmer plots for ClO^- quenching by N-CQDs at different temperatures

caused by ClO^- is attributed to the dynamic quenching mechanism (Bandi et al. 2018; Bunkoed & Kanatharana 2015). This result contrasts many findings that reported fluorophore quenching by ClO^- to be caused primarily by static quenching (Duan et al. 2015; Yuan et al. 2016). This is explained by the oxidative properties of the ion that causes the formation of non-radiative complexes between the fluorophore and quencher (ClO^-). However, the report of dynamic quenching by ClO^- is yet to be reported.

As such, we proposed a possible mechanism that dynamic quenching could occur. Dynamic quenching by heavy atom halogens (Cl, Br, and I) and halogen-containing molecules are known to be the result of intersystem crossing, facilitated by the heavy atom effect (Geddes et al. 2001; Lakowicz 1999). Hence, ClO^- may be considered to have these properties. Intersystem crossing occurs when a collision of a quencher with a fluorophore causes the excited singlet state of the fluorophore to become an excited triplet. The heavy atom effect involves the presence of an atom with a high atomic number that enhances the rate of spin-forbidden process of the N-CQDs, allowing intersystem crossing to occur (Braslavsky 2007). This mechanism plays a crucial role in the non-radiative deactivation of the N-CQDs as the excited electron of the N-CQDs returns to the ground state by non-radiative decay from its excited triplet state (Lakowicz 2006; Reichardt et al. 2013). Figure 11 illustrates the possible dynamic quenching mechanism of N-CQDs by ClO^-.

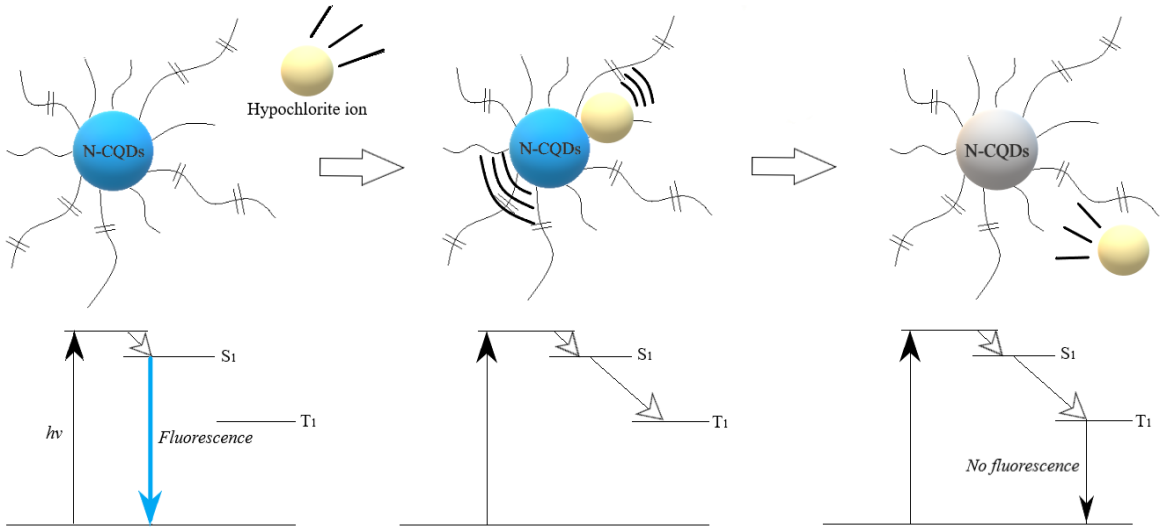

FIGURE 11. Possible dynamic quenching mechanism of N-CQDs by ClO^-

CONCLUSION

This study demonstrated a facile microwave synthesis method for the preparation of N-CQDs with a quantum yield of 14.8%, using citric acid monohydrate (CA) and urea. The as-synthesised N-CQDs with an average particle size of 7.29 ± 3.91 nm were non-toxic, reproducible, have a high-intensity blue fluorescence emission and exhibited excitation-independent fluorescence emission. The excitation-independent fluorescence emission was caused by surface-state-induced fluorescence. It was found that free chlorine (in the form of ClO^-) was successfully detected using the optimised N-CQDs at pH 9 after 30 min, providing a LOD of 0.4 mM and a of 1.2 mM. The detection was concluded to be high range, precise and accurate due to a moderate intra-day and inter-day precision and acceptable recovery, which makes the N-CQDs suitable to be used for wastewater testing. Furthermore, the FL quenching process of N-CQDs upon spiking with ClO^- was caused by dynamic quenching, which is a result worth further research. The N-CQDs were also proven to have high selectivity towards free chlorine, compared to other ions

commonly found in wastewater. Hence, the microwave synthesis of N-CQDs in this study could be useful in environmental science as a fluorescent probe for free chlorine detection.

ACKNOWLEDGEMENTS

This research work was supported by the Ministry of Higher Education, Malaysia for Fundamental Research Grant Scheme with Project Code (FRGS/1/2019/STG07/USM/02/17). The work is also financially supported by USM Research University Individual Grant (1001/PKimia/8011086). There are no conflicts to declare.

REFERENCES

Bandi, R., Dadigala, R., Gangapuram, B.R. & Guttena, V. 2018. Green synthesis of highly fluorescent nitrogen–doped carbon dots from *Lantana camara* berries for effective detection of lead (II) and bioimaging. *Journal of Photochemistry and Photobiology B: Biology* 178: 330-338.

Braslavsky, S.E. 2007. Glossary of terms used in photochemistry (IUPAC Recommendations 2006). *Pure and Applied Chemistry* 79(3): 293-465.

Bunkoed, O. & Kanatharana, P. 2015. Mercaptopropionic acid capped CdTe quantum dots as fluorescence probe for the determination of salicylic acid in pharmaceutical products. *Luminescence* 30(7): 1083-1089.

Chen, P., Wei, W.Z. & Yao, S.Z. 1999. Different valency chlorine species analysis by non-suppressed ion-chromatography with double cell quartz crystal detector. *Talanta* 49(3): 571-576.

Crook, J., Ammerman, D., Okun, D. & Matthews, R. 2012. *EPA Guidelines for Water Reuse.* p.643.

de Medeiros, T.V., Manioudakis, J., Noun, F., Macairan, J.R., Victoria, F. & Naccache, R. 2019. Microwave-assisted synthesis of carbon dots and their applications. *Journal of Materials Chemistry C* 7(24): 7175-7195.

Ding, H. & Xiong, H.M. 2015. Exploring the blue luminescence origin of nitrogen-doped carbon dots by controlling the water amount in synthesis. *RSC Advances* 5(82): 66528-66533.

Ding, H., Yu, S.B., Wei, J.S. & Xiong, H.M. 2016. Full-color light-emitting carbon dots with a surface-state-controlled luminescence mechanism. *ACS Nano* 10(1): 484-491.

Du, Y. & Guo, S. 2016. Chemically doped fluorescent carbon and graphene quantum dots for bioimaging, sensor, catalytic and photoelectronic applications. *Nanoscale* 8(5): 2532-2543.

Duan, R., Li, C., Liu, S., Liu, Z., Li, Y., Zhu, J. & Hu, X. 2015. A selective fluorescence quenching method for the determination of trace hypochlorite in water samples with nile blue A. *Journal of the Taiwan Institute of Chemical Engineers* 50: 43-48.

Emmanuel, E., Keck, G., Blanchard, J.M., Vermande, P. & Perrodin, Y. 2004. Toxicological effects of disinfections using sodium hypochlorite on aquatic organisms and its contribution to AOX formation in hospital wastewater. *Environment International* 30(7): 891-900.

Geddes, C.D., Apperson, K., Karolin, J. & Birch, D.J. 2001. Chloride-sensitive fluorescent indicators. *Analytical Biochemistry* 293(1): 60-66.

Hallaj, T., Amjadi, M., Manzoori, J.L. & Shokri, R. 2015. Chemiluminescence reaction of glucose-derived graphene quantum dots with hypochlorite, and its application to the determination of free chlorine. *Microchimica Acta* 182(3): 789-796.

Heidelberger, M. & Treffers, H.P. 1942. Quantitative chemical studies on hemolysins: I. The estimation of total antibody in antisera to sheep erythrocytes and stromata. *The Journal of General Physiology* 25(4): 523.

Hussain, S.N., Asghar, H.M.A., Sattar, H., Brown, N.W. & Roberts, E.P.L. 2015. Free chlorine formation during electrochemical regeneration of a graphite intercalation compound adsorbent used for wastewater treatment. *Journal of Applied Electrochemistry* 45(6): 611-621.

Kaasalainen, M., Aseyev, V., von Haartman, E., Karaman, D.Ş., Mäkilä, E., Tenhu, H., Rosenholm, J. & Salonen, J. 2017. Size, stability, and porosity of mesoporous nanoparticles characterized with light scattering. *Nanoscale Research Letters* 12: 74.

Kalaiyarasan, G., Hemlata, C. & Joseph, J. 2019. Fluorescence turn-on, specific detection of cystine in human blood plasma and urine samples by nitrogen-doped carbon quantum dots. *ACS Omega* 4(1): 1007-1014.

Kim, T.H., Ho, H.W., Brown, C.L., Cresswell, S.L. & Li, Q. 2015. Amine-rich carbon nanodots as a fluorescence probe for methamphetamine precursors. *Analytical Methods* 7(16): 6869-6876.

Koide, Y., Urano, Y., Hanaoka, K., Terai, T. & Nagano, T. 2011. Development of an Si-rhodamine-based far-red to near-infrared fluorescence probe selective for hypochlorous acid and its applications for biological imaging. *Journal of the American Chemical Society* 133(15): 5680-5682.

Lakowicz, J.R. 2006. Mechanisms and dynamics of fluorescence quenching. In *Principles of Fluorescence Spectroscopy.* Boston: Springer. pp. 331-351.

Lakowicz, J.R. 1999. Quenching of fluorescence. In *Principles of Fluorescence Spectroscopy.* Boston: Springer. pp. 237-265.

Liu, M.L., Chen, B.B., Li, C.M. & Huang, C.Z. 2019. Carbon dots: Synthesis, formation mechanism, fluorescence origin and sensing applications. *Green Chemistry* 21(3): 449-471.

Liu, W., Li, C., Sun, X., Pan, W., Yu, G. & Wang, J. 2017. Highly crystalline carbon dots from fresh tomato: UV emission and quantum confinement. *Nanotechnology* 28(48): 485705.

Lou, Z., Li, P. & Han, K. 2015. Redox-responsive fluorescent probes with different design strategies. *Accounts of Chemical Research* 48(5): 1358-1368.

Malvern Panalytical Ltd. 2018. *Dynamic Light Scattering: An Introduction in 30 Minutes.* Technical Note (MRK656-01). pp. 1-8.

National Institute for Occupational Safety and Health (NIOSH). 1997. *Pocket Guide to Chemical Hazards*. U.S. Department of Health and Human Services, Public Health Service, Centers for Disease Control and Prevention, Cincinnati, OH.

Pobozy, E., Pyrzynska, K., Szostek, B. & Trojanowicz, M. 1995. Flow-injection spectrophotometric determination of free residual chlorine in waters with 3, 3′-dimethylnaphtidine. *Microchemical Journal* 51(3): 379-386.

Qin, J., Zhang, L. & Yang, R. 2019. Solid pyrolysis synthesis of excitation-independent emission carbon dots and its application to isoniazid detection. *Journal of Nanoparticle Research* 21: 59.

Qu, D., Zheng, M., Li, J., Xie, Z. & Sun, Z. 2015. Tailoring color emissions from N-doped graphene quantum dots for bioimaging applications. *Light: Science and Applications* 4(12): e364-e364.

Reichardt, C., Wen, C., Vogt, R.A. & Crespo-Hernández, C.E. 2013. Role of intersystem crossing in the fluorescence quenching of 2-aminopurine 2'-deoxyriboside in solution. *Photochemical and Photobiological Sciences* 12(8): 1341-1350.

Shanmugaraj, K. & Ilanchelian, M. 2017. Visual and optical detection of hypochlorite in water samples based on etching of gold/silver alloy nanoparticles. *New Journal of Chemistry* 41(23): 4130-14136.

Shepherd, J., Hilderbrand, S.A., Waterman, P., Heinecke, J.W., Weissleder, R. & Libby, P. 2007. A fluorescent probe for the detection of myeloperoxidase activity in atherosclerosis-associated macrophages. *Chemistry and Biology* 14(11): 1221-1231.

Simões, E.F., Leitão, J.M. & da Silva, J.C. 2016. Carbon dots prepared from citric acid and urea as fluorescent probes for hypochlorite and peroxynitrite. *Microchimica Acta* 183(5): 1769-1777.

Song, Y., Zhu, S., Xiang, S., Zhao, X., Zhang, J., Zhang, H., Fu, Y. & Yang, B. 2014. Investigation into the fluorescence quenching behaviors and applications of carbon dots. *Nanoscale* 6(9): 4676-4682.

Sun, Z., Li, X., Wu, Y., Wei, C. & Zeng, H. 2018. Origin of green luminescence in carbon quantum dots: Specific emission bands originate from oxidized carbon groups. *New Journal of Chemistry* 42(6): 4603-4611.

Wakigawa, K., Gohda, A., Fukushima, S., Mori, T., Niidome, T. & Katayama, Y. 2013. Rapid and selective determination of free chlorine in aqueous solution using electrophilic addition to styrene by gas chromatography/mass spectrometry. *Talanta* 103: 81-85.

Wang, B. & Anzai, J.I. 2015. A facile electrochemical detection of hypochlorite ion based on ferrocene compounds. *International Journal of Electrochemical Science* 10(4): 3260-3268.

Wang, T., Wang, A., Wang, R., Liu, Z., Sun, Y., Shan, G., Chen, Y. & Liu, Y. 2019. Carbon dots with molecular fluorescence and their application as a "turn-off" fluorescent probe for ferricyanide detection. *Scientific Reports* 9(1): 1-9.

Watanabe, T., Idehara, T., Yoshimura, Y. & Nakazawa, H. 1998. Simultaneous determination of chlorine dioxide and hypochlorite in water by high-performance liquid chromatography. *Journal of Chromatography A* 796(2): 397-400.

Xia, C., Tao, S., Zhu, S., Song, Y., Feng, T., Zeng, Q., Liu, J. & Yang, B. 2018. Hydrothermal addition polymerization for ultrahigh-yield carbonized polymer dots with room temperature phosphorescence via nanocomposite. *Chemistry - A European Journal* 24(44): 11303-11308.

Xia, C., Zhu, S., Feng, T., Yang, M. & Yang, B. 2019. Evolution and synthesis of carbon dots: From carbon dots to carbonized polymer dots. *Advanced Science* 6(23): 1901316.

Yadav, R., Odera, K., Rai, A., Noguchi, A., Takahashi, R. & Mishra, L. 2019. A stable and highly sensitive fluorescent probe for detection of hypochlorite ion *in vitro* and in living cells. *Chemistry Letters* 48(2): 110-113.

Yan, F., Sun, Z., Zhang, H., Sun, X., Jiang, Y. & Bai, Z. 2019. The fluorescence mechanism of carbon dots, and methods for tuning their emission color: A review. *Microchimica Acta* 186(8): 583.

Yee, L.F., Abdullah, M.P., Ata, S. & Ishak, B. 2006. Dissolved organic matter and its impact on the chlorine demand of treated water. *Malaysian Journal of Analytical Sciences* 10(2): 243-250.

Yoo, D., Park, Y., Cheon, B. & Park, M.H. 2019. Carbon dots as an effective fluorescent sensing platform for metal ion detection. *Nanoscale Research Letters* 14(1): 1-13.

Yu, W.W., Qu, L., Guo, W. & Peng, X. 2003. Experimental determination of the extinction coefficient of CdTe, CdSe, and CdS nanocrystals. *Chemistry of Materials* 15(14): 2854-2860.

Yuan, Y., Huang, X., Liu, S., Yang, J., Duan, R. & Hu, X. 2016. Determination of hypochlorite by quenching the fluorescence of 1-pyrenylboronic acid in tap water. *RSC Advances* 6(4): 3393-3398.

Zhang, Y., He, Y.H., Cui, P.P., Feng, X.T., Chen, L., Yang, Y.Z. & Liu, X.G. 2015. Water-soluble, nitrogen-doped fluorescent carbon dots for highly sensitive and selective detection of Hg 2+ in aqueous solution. *RSC Advances* 5(50): 40393-40401.

Zhao, P. & Zhu, L. 2018. Dispersibility of carbon dots in aqueous and/or organic solvents. *Chemical Communications* 54(43): 5401-5406.

Zu, F., Yan, F., Bai, Z., Xu, J., Wang, Y., Huang, Y. & Zhou, X. 2017. The quenching of the fluorescence of carbon dots: A review on mechanisms and applications. *Microchimica Acta* 184(7): 1899-1914.

Zulfajri, M., Dayalan, S., Li, W.Y., Chang, C.J., Chang, Y.P. & Huang, G.G. 2019. Nitrogen-doped carbon dots from *Averrhoa carambola* fruit extract as a fluorescent probe for methyl orange. *Sensors* 19(22): 5008.

*Corresponding author; email: hllee@usm.my